PCCP

ROYAL SOCIETY OF CHEMISTRY

PAPER

View Article Online
View Journal

Cite this: DOI: 10.1039/d2cp05500g

Thermodynamic stability of Li–B–C compounds from first principles†

Saba Kharabadze, [a] Maxwell Meyers,[a] Charlsey R. Tomassetti, [a] Elena R. Margine, [a] Igor I. Mazin[bc] and Aleksey N. Kolmogorov *[a]

Received 24th November 2022,
Accepted 6th February 2023

DOI: 10.1039/d2cp05500g

rsc.li/pccp

Prediction of high-T_c superconductivity in hole-doped Li_xBC two decades ago has brought about an extensive effort to synthesize new materials with honeycomb B–C layers, but the thermodynamic stability of Li–B–C compounds remains largely unexplored. In this study, we use density functional theory to characterize well-established and recently reported Li–B–C phases. Our calculation of the Li chemical potential in Li_xBC helps estimate the (T,P) conditions required for delithiation of the LiBC parent material, while examination of B–C phases helps rationalize the observation of metastable BC_3 polymorphs with honeycomb and diamond-like morphologies. At the same time, we demonstrate that recently reported BC_3, $LiBC_3$, and Li_2B_2C phases with new crystal structures are both dynamically and thermodynamically unstable. With a combination of evolutionary optimization and rational design, we identify considerably more natural and favorable Li_2B_2C configurations that, nevertheless, remain above the thermodynamic stability threshold.

1 Introduction

The combination of low atomic mass and strong covalent bonding makes binary and ternary Li–B–C compounds suitable for a variety of practical applications. The $B_{4-6.5}C$ ceramic with outstanding Vickers hardness and high thermal stability has found uses as a protective material.[1] Li-intercalated graphite compounds with the 372 mA h g^{-1} theoretical specific capacity have served as anodes in commercial Li-ion batteries.[2] The presence of high-frequency phonon modes and hole-doped electronic states makes Li–B–C materials with honeycomb layers particularly promising conventional superconductors with high critical temperatures (T_c). For example, our *ab initio* re-examination of a recently synthesized LiB has indicated that the material's T_c could exceed 32 K.[3] One of the most tantalizing predictions by Rosner *et al.* in 2002[4] was the possibility of obtaining $Li_{x\approx0.5}BC$ superconductors that could operate at temperatures above liquid nitrogen. However, the following synthesis and detailed characterization of the targeted delithiated Li_xBC material revealed no signs of superconductivity.[5–8] The search for new Li–B–C materials has continued in recent years and resulted in reports of new Li_2B_2C,[9] BC_3,[10] and $LiBC_3$[11] phases with unique crystal structures.

Key Li–B–C materials observed under ambient conditions are summarized in Fig. 1. The Li–B binary features Li_3B_{14} and LiB_3 compounds with intercalated B frameworks,[12] an unusual $LiB_{x\approx0.9}$ compound with linear B chains,[13,14] and a predicted LiB with B layers synthesized *via* cold compression and annealed to 1 bar.[15,16] The Li–C system includes LiC_{6n} (n = 1, 2) phases of Li-intercalated graphite, LiC with C_2 dimers, and Li_4C_3 with C_3 trimers.[17–19] The B–C binary contains $B_{4-6.5}C$ related to pure B phases and different BC_3 polymorphs with 2D and 3D B–C frameworks.[20–22] The well-established ternary compounds are $LiB_{13}C_2$ and LiB_6C with linked B_{12} icosahedra[23] and the layered LiBC[24] with its delithiated Li_xBC derivatives ($x > 0.38$).[5–7] While the three binary systems have been the subject of several comprehensive *ab initio* modeling studies,[14,19,25] the thermodynamic stability of the Li–B–C ternary compounds has not yet been investigated systematically.

In this density functional theory (DFT) study, we focus on analyzing the stability of published structural models for Li–B–C compounds. Firstly, we evaluate temperatures and Li_2^{gas} vapor pressures needed to trigger the delithiation of LiBC. The constructed phase diagram for this process is shown to be consistent with the typical synthesis conditions used in experiments.[5,7] Secondly, we calculate the formation energies of B–C phases across a wide composition range to rationalize the observation of B-rich and C-rich materials. The observed BC_3 phases with layered[21] or diamond-like[22] morphologies are confirmed to be

[a] Department of Physics, Applied Physics and Astronomy, Binghamton University, State University of New York, PO Box 6000, Binghamton, New York 13902-6000, USA. E-mail: kolmogorov@binghamton.edu
[b] Department of Physics and Astronomy, George Mason University, Fairfax, Virginia 22030, USA
[c] Quantum Science and Engineering Center, George Mason University, Fairfax, Virginia 22030, USA

† Electronic supplementary information (ESI) available. See DOI: https://doi.org/10.1039/d2cp05500g

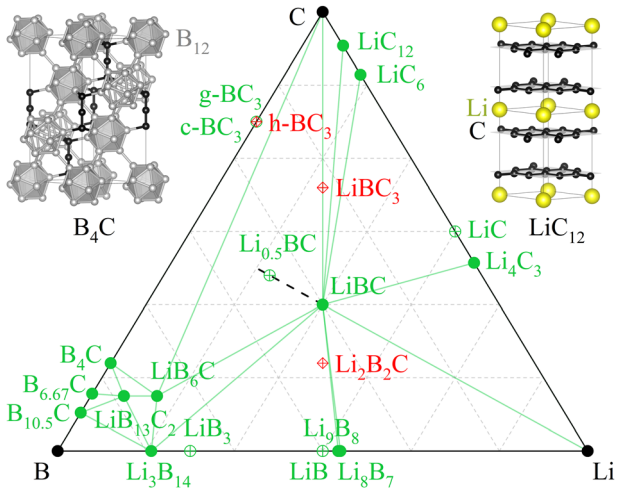

Fig. 1 Convex hull of Li–B–C compounds determined with DFT (optB86b-vdW) calculations at T = 0 K. Observed compounds found to be stable and metastable in this approximation are shown with solid and crossed green circles, respectively. Previously reported phases determined in this study to be unstable are displayed with crossed red circles. The dashed black line shows the observed stability range of Li_xBC phases. The morphology of the B_4C compound is shown with a simplified ordered metastable structure.

only metastable,[20] which explains the need for the employed precursor-based synthesis routes. On the other hand, we show that the newest BC_3 polymorph, h-BC_3, comprised of alternating BC and C layers,[10] is highly unstable thermodynamically and appears to be an unlikely product of reaction between elemental B and C. Thirdly, we determine that the reported $LiBC_3$ phase in the form of intercalated h-BC_3[11] is a similarly unstable configuration. Finally, we show a number of unnatural features in the proposed structural model for the synthesized Li_2B_2C.[9] We identify considerably more favorable configurations that remain only metastable. Our findings reveal an incomplete knowledge of the Li–B–C ternary and the need for further experimental exploration of this intriguing materials system.

2 Methodology

All DFT calculations were performed with the Vienna *ab initio* simulation package (VASP).[26–29] The energy cutoff of 500 eV and dense ($\Delta k \sim 0.02$ Å^{-1}) Monkhorst–Pack k-point meshes[30] ensured good numerical convergence of relative energies. All structures were fully relaxed with the EDIFFG = −0.005 tolerance, which led to the convergence of energies, forces, and stresses to typically below ∼1 meV per atom, 0.005 eV Å^{-1}, and 1 kB, respectively. Unless specified otherwise, we used the nonlocal van der Waals (vdW) functional optB86b-vdW.[31] Select phases were examined with the generalized gradient approximation-based Perdue–Burke–Ernzerhof (PBE) exchange-correlation functional[32,33] or within the local density approximation (LDA).[34,35] The vdW-corrected functional was employed to account for dispersive interactions that play an important role for structural and bonding properties in layered Li–B–C materials. For instance, it allowed us to show that the disagreements between previously observed and our calculated interlayer distances in recently reported h-BC_3 and h-$LiBC_3$ polymorphs exceed the expected DFT errors. Formation energies of Li–C binary compounds have also been previously shown to be particularly sensitive to the systematic DFT errors.[19] In our optB86b-vdW calculations, LiC is metastable at low temperatures but becomes thermodynamically stable around 300 K upon inclusion of the vibrational entropy. LiB_3 is also expected to stabilize at high temperatures.[3]

Global structure searches at specific Li–B–C compositions relied on an evolutionary algorithm implemented in the module for *ab initio* structure evolution MAISE.[36] Populations of 16–20 structures with up to 20 atoms were generated randomly and evolved with our standard mutation and crossover operations[36] for 20–50 generations. The thermodynamic corrections due to vibrational entropy were evaluated within the finite displacement method implemented in PHONOPY.[37] We used supercells with at least 80 atoms and applied 0.1 Å displacements within the harmonic approximation. While the zero point energy (ZPE) is known to have a sizable magnitude in light materials, ranging from 40 meV per atom in bcc-Li to 171 meV per atom in graphite in our calculations, Table S1 (ESI†) shows that it canceled out effectively in the evaluation of formation energies and did not change the stability ordering for any of the considered phases. Since some of the Li–B–C structures were too large for phonon calculations or found to be dynamically unstable, we used energies in all the relative stability plots but showed values corrected with the ZPE and the vibrational entropy term at T = 600 K for key materials in Table S1 (ESI†). We also examined the importance of anharmonic effects at high temperatures using the quasi-harmonic approximation (QHA). Detailed structural information for relevant phases considered in this study is given in the ESI.†

3 Results and discussion

3.1 Li_xBC

Wörle *et al.* first observed the formation of semiconducting LiBC in 1995.[24] Particular interest in the layered compound was spurred by early 2000s computational studies suggesting the material's potential for high-T_c superconductivity in a hole-doped form.[4,38] In the following few years, a number of different methods were used to obtain phases with reduced Li content, from delithiation of LiBC *via* vacuum annealing[5,39] or oxidation in organic solvents[6] to direct synthesis of Li_xBC by varying the starting fluxes.[40,41] The resulting compounds were obtained in a wide range of x, but those in the low Li regime ($x < 0.5$) were difficult to characterize, being highly disordered, multiphasic, amorphous, or with significant impurities.[6,39,40] The low crystallinity of these Li-poor samples pointed towards a thermodynamic limit to the reduction of Li in LiBC. A later experimental study by Fogg *et al.*[7] reported several critical concentrations where severe alterations in the LiBC structure were observed, including the swapping of B/C sites with the consequent formation of C–C and B–B bonds below $x \approx 0.55$ and the expulsion of B below $x \approx 0.45$. Detailed X-ray and neutron powder

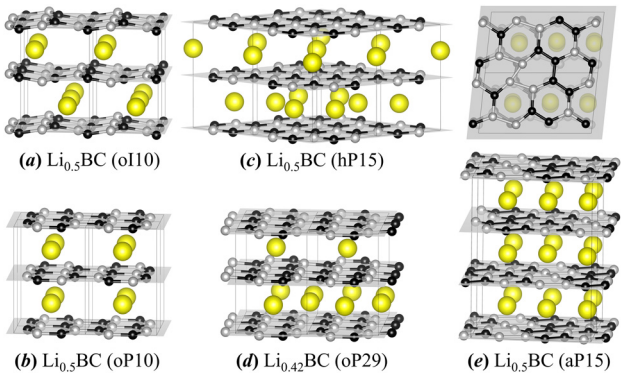

Fig. 2 Simulated structural Li_xBC models at or near x = 0.5. Phases (a)–(d) have uniformly ordered BC honeycomb layers and different populations of Li sites. The most stable aP15-$Li_{0.5}BC$ polymorph (e) found in our evolutionary searches has a distorted BC network with C–C and B–B bonds.

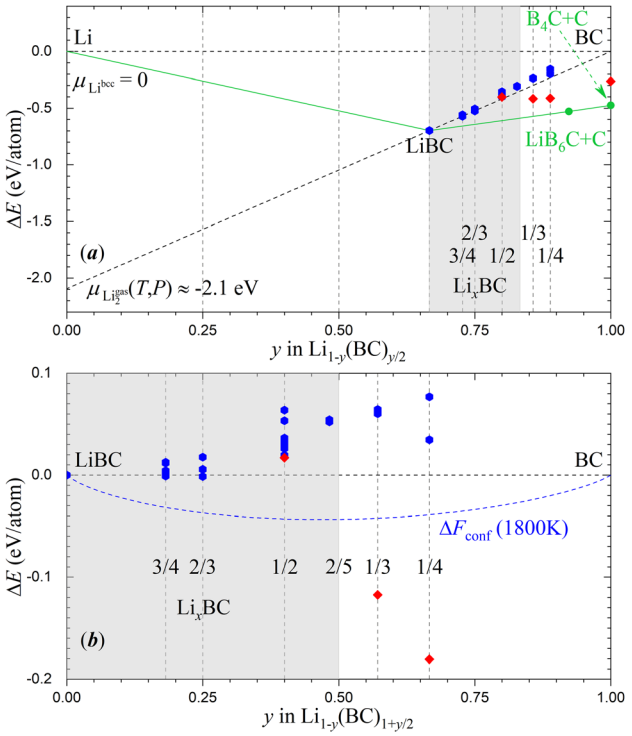

Fig. 3 Relative energies of Li_xBC pseudobinary phases referenced to (a) bcc-Li and layered BC or (b) LiBC and layered BC. The blue hexagons and red diamonds denote phases with honeycomb BC layers and general morphologies found with evolutionary searches, respectively. The green lines define the convex hull. The blue dashed line in (b) shows the configurational entropy contribution to the free energy for Li_xBC at 1800 K. The shaded region marks experimentally observed compositions.

diffraction characterization of the obtained samples with x = 0.16–0.36 nominal compositions indicated the formation of C-rich ternary and B-rich binary phases, *e.g.*, $Li_{0.21(1)}B_{0.73(1)}C_{1.27(1)}$ and $B_{13}C_2$ phases at x = 0.16. The idea of an upper limit to LiBC delithiation is further supported with DFT calculations[7] and by the most recent findings by Kalkan and Ozdas[8] who synthesized samples with Daumas–Hérold-type domains of Li_xBC in the $0.43 \leq x \leq 0.85$ range.

The successful Li_xBC synthesis work has been followed by detailed measurements of materials' various properties.[5–8,42] Unfortunately, no superconductivity in Li_xBC has been detected in any of these studies, although Li reduction in LiBC has been shown to increase conductivity.[5,7,8] While *ab initio* studies of LiBC and its derivatives have examined the materials' bonding, superconducting, electrochemical, and other properties,[7,42–47] the thermodynamics of the Li_xBC formation appears to be not fully explored.

We began our investigation by screening the $0.25 \leq x \leq 0.75$ pseudobinary range for favorable configurations using two complementing approaches. First, we systematically scanned all possible decorations of Li sites in LiBC supercells with up to 18 atoms and optimized the candidate structures (Fig. 2). The formation energies of the best layered phases ended up well above the convex hull at T = 0 K defined by combination of LiBC and the mixture of the pure C and LiB_6C materials (Fig. 3(a)) but fairly close to the line defined by the observed fully occupied and hypothetical fully delithiated compounds with the B–C frameworks (Fig. 3(b)). Different population of Li sites was found to disperse the energy by a sizable 45 meV per atom. At x = 0.5, for example, structures with uniform distributions of Li atoms that broke the hexagonal symmetry and led to a noticeable buckling of the BC layers (Fig. 2(a) and (b)) were more favorable by at least 4.5 meV per atom than the hexagonal configuration with an uneven 2 : 1 population of sites in adjacent layers (Fig. 2(c)). Nevertheless, the kinetics of the deintercalation process may favor unequal populations as shown with the off-stoichiometry $Li_{0.42}BC$ prototype (Fig. 2(d)) that approximates the experimentally observed decoration.[8]

Second, we performed evolutionary searches starting from random structures to explore configurations beyond the familiar layered morphologies. While the global optimization runs found the honeycomb frameworks to be lowest-energy minima for $x >$ 0.5, different motifs started to emerge at lower Li concentrations. At x = 0.5, the low-symmetry structure with swapped B and C atoms causing a severe hexagon distortion at B sites (Fig. 2(d)), a pattern similar to the one observed in previous DFT simulations,[7] turned out to be slightly favored, by 2 meV per atom, over all considered LiBC derivatives. At smaller x = 1/3, 1/4, and 0 values, 3D frameworks comprised of sp^2 and/or sp^3 sites became dominant and lowered the energy by over 100 meV per atom. These findings are in line with the experimental observations regarding the delithiation limit, the defect types, and the lack of Li_xBC stability at T = 0 K.

In order to account for the temperature-dependent factors determining the thermodynamics of the delithiation process, we evaluated the entropic terms in the Gibbs free energy for relevant Li-containing solid and gas phases. The configurational entropy of Li in disordered Li_xBC can be approximated assuming equiprobable occurrence of different decorations. The $\Delta F_{conf} = kT[x\ln(x) + (1 - x)\ln(1 - x)]/(2 + x)$ contribution factoring in a variable number of Li atoms per formula unit is shown as a function of $y = (1 - x)/(1 + x/2)$ in Fig. 3(b). The correction brings the free energy of intermediate phases below

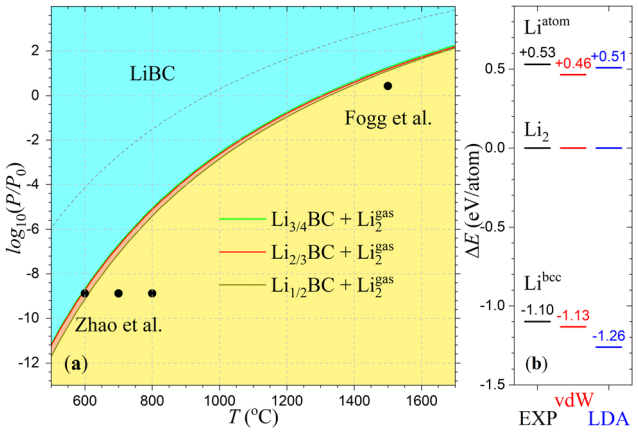

Fig. 4 (a) Calculated (*T*,*P*) phase boundary between ordered LiBC and $Li_xBC + Li_2^{gas}$ mixtures (solid lines) along with reported Li_xBC synthesis conditions (circles).[5,7] The gray dashed line corresponds to a kinetically inaccessible phase transition between LiBC and $C + B_4C + Li_2^{gas}$. (b) Relative energy of Li referenced to the atomic energy of the Li_2 molecule, with experimental values taken from ref. 48 and 49 (see Table S2, ESI† for more details).

the LiBC ↔ BC tie-line but is insufficient to stabilize them with respect to the convex hull even at 1800 K. The vibrational contribution evaluated within the harmonic approximation has a similar effect on Li_xBC stability. For example, the free energy distances to the LiBC ↔ (C + B_4C) tie-line at 1800 K for the ordered hP8-$Li_{2/3}BC$ and oI10-$Li_{0.5}BC$ changed from +118 to +99 meV per atom and from +210 to +175 meV per atom, respectively.

An unsurprising conclusion is that the deintercalation must be governed by the substantial entropy Li gains in its diatomic gas state. This contribution can be evaluated using calculated quantities for the vibrational, rotational, and translational degrees of freedom within the ideal diatomic gas model[48] (see ESI†). Fig. 3(a) illustrates that for LiBC to become thermodynamically unstable, the chemical potential of Li_2^{gas} has to drop below a linearly extrapolated free energy value between the free energies of Li_xBC and LiBC for at least one *x*. Since *ab initio* computation of the configurational and vibrational contributions for disordered phases is computationally challenging, we relied on the observed trend that the relative free energies of the Li_xBC phases lie within ~20 meV per atom to the LiBC ↔ BC tie-line.

We estimated the location of the *x*-dependent phase boundaries using representative ordered oS44, hP8, and oI10 structures at $x = 3/4$, 2/3, and 1/2, respectively. Once the vibrational entropy was included, we calculated the equilibrium (*T*,*P*) values in the 800–2000 K range by matching the Gibbs free energies per Li atom for LiBC and the three mixtures of Li_xBC and Li_2^{gas}. The corresponding stability domains are plotted in Fig. 4(a). We also considered a possible full decomposition of LiBC into Li_2^{gas} + C + B_4C (a slightly more stable combination than Li_2^{gas} + C + LiB_6C at elevated temperatures) shown with a gray dashed line. Thermodynamically, this transformation should happen first upon heating LiBC and/or reducing the Li_2^{gas} vapor pressure and prevent the formation of any Li_xBC derivatives but, kinetically, it is evidently hindered by the high barriers associated with breaking the strong covalent B–C bonds. The presence of some metastable products makes the constructed phase diagram transitional.[49]

To gauge the sensitivity of the phase boundaries to systematic DFT errors, we compared the calculated and measured energies of the spin-polarized atomic, diatomic, and bcc Li (Fig. 4(b)).[50,51] The slight overbinding of bcc-Li with respect to molecular Li_2 by 0.03 eV per Li in our default DFT approximation would result in a small shift in the boundary, $\Delta \log_{10}(P/P_0) \approx 0.03/0.07 \log_{10}(e) \approx 0.19$ at 800 K. Assessment of discrepancies between DFT and experiment for solid state phases is more challenging because measurements are usually conducted at elevated temperatures.[52] The typical differences of up to ~20 meV per atom between DFT flavors in the calculation of relative energies[3,12,52] and the neglected configurational entropy term of similar values (Fig. 3(b)) could be amplified to a sizable 0.2 eV per Li upon rescaling to be per Li atom. This could lead to up to an order of magnitude change in the estimate of the transition pressure.

We also performed QHA calculations to check how volume expansion affects the free energies of LiBC and $Li_{0.5}BC$ at highest temperatures used in the delithiation experiments. As shown in Fig. S1 and S2 (ESI†), the minimum of $F(T,V)$ shifts by −21.53 meV per atom and −23.16 meV per atom at 1800 K, respectively, once the two phases are allowed to expand. This results in a −13.4 meV per Li change in the Gibbs free energy difference that defines the phase boundary between $Li_2B_2C_2$ and $1/2Li_2 + LiB_2C_2$. Other anharmonic terms for molecules and solids are much harder to evaluate from first principles.[53–56] Given the relatively small value of the QHA corrections compared to the uncertainties estimated above, the use of the harmonic approximation seems fitting in this case.

The reliability of the proposed phase diagram can be checked against explicitly specified synthesis conditions in two previous studies.[5,7] Zhao *et al.*[5] carried out LiBC deintercalation at three relatively low temperatures maintaining a 10^{-6} torr vacuum. The 12 hour experiments at 600, 700, and 800 °C were estimated to reduce the Li content down to $x = 0.80$, 0.77, and 0.63, respectively. Fogg *et al.*[7] performed deintercalation at higher $T = 1500$ °C and estimated the Li_2^{gas} vapor partial pressure to be 2.7 atm using the Clausius–Clapeyron equation. Based on a series of experiments for durations between 1 and 24 hours which led to different *x* values, the authors concluded that it is difficult to control the precise amount of Li in these dynamic non-equilibrium reactions.

The reported Li deintercalation (*T*,*P*) conditions fall appropriately outside of our calculated LiBC stability domain (Fig. 4(a)). The narrowness of the estimated stability regions for intermediate *x* values suggests that the targeted *x* values may indeed be easier to obtain by relying on the kinetics (*e.g.*, tuning the duration and temperature profile of the deintercalation process) rather than thermodynamics (*i.e.*, trying to pinpoint suitable (*T*,*P*) conditions).

3.2 BC_3

Determination of the B-rich part of the B–C phase diagram has required several iterations.[20,57–64] Originally identified as

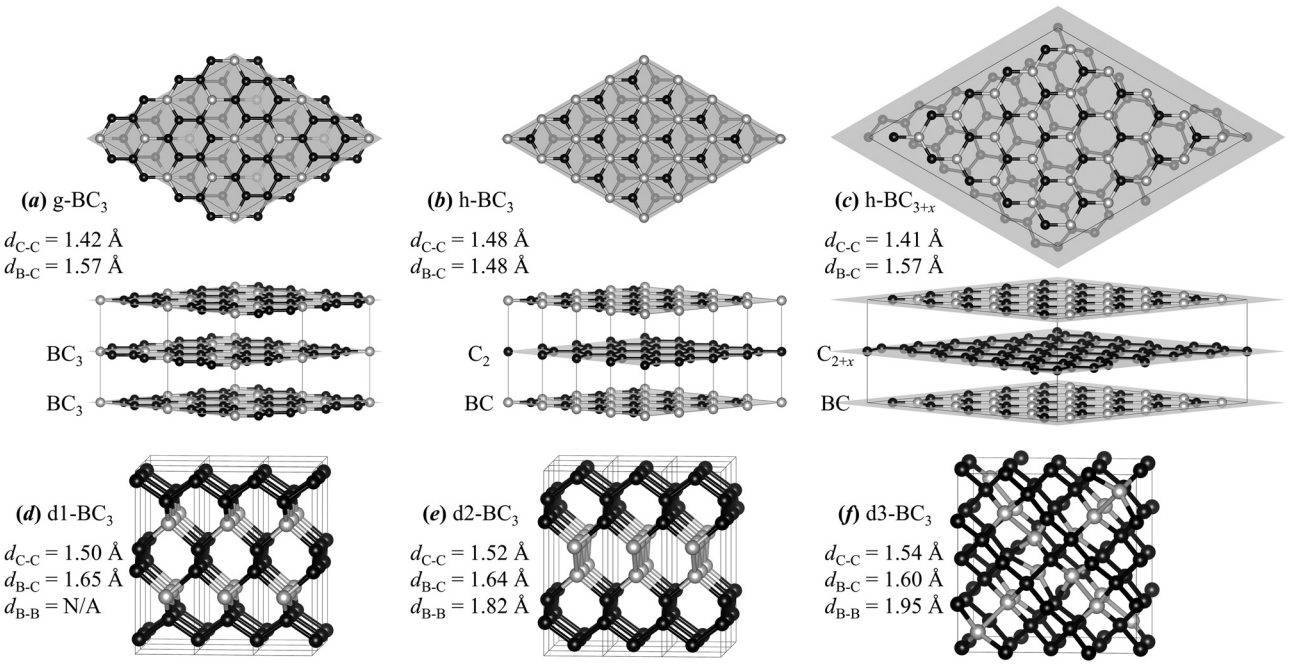

Fig. 5 Select structures with sp^2 (a)–(c) or sp^3 (d)–(f) bonding at or near the BC_3 composition. (a), (b), (f) Previously proposed models explaining experimentally observed phases. (c) A hybrid h-BC_{3+x} unit cell with natural B–C and C–C bond lengths achieved by twisting BC and C_2 layers.

related but distinct hR45-$B_{13}C_2$[65] and hR45-B_4C[66] compounds with the $R\bar{3}m$ symmetry, they have been ultimately found to be a single $B_{4+\delta}C$ intermediate phase with a large homogeneous region of $(0.088 < x \leq 0.2)$ in $B_{1-x}C_x$. The composition variability arises from the thermodynamic favorability of connecting the B_{12} icosahedra with different blocks.[67–70] In our study, we use B_4C,[68,69,71] $B_{6.67}C$,[25] and $B_{10.5}C$[25] models that fall into the stability range at low temperatures. The first one was constructed as CBC-$B_{11}C^p$ with a C atom populating a polar site in B_{12} and a B atom populating the mid-point site in three-atom chains shown in Fig. 1. The last two B-rich representative structures were obtained by expanding the hR45-$B_{13}C_2$ primitive unit cell and distributing $B\left\langle \begin{matrix} B \\ B \end{matrix} \right\rangle B$ (OPO1) or CBC$\cdots$B (OPO2) blocks in the $3 \times 3 \times 3$ supercell as described in ref. 25 (see ESI† for more details). We note that the tie-lines defined by the $B_{4+\delta}C$ phase have little bearing on the stability of the BC_3 polymorphs known to have large positive formation energies.[25,72]

The feasibility of synthesizing a borocarbide at the 1 : 3 composition was demonstrated by Kouvetakis *et al.* in 1986.[21] A metastable graphite-like g-BC_3 phase was obtained *via* a chemical vapor deposition reaction of $2BCl_3$ with C_6H_6 at 800 °C yielding $2BC_3$ and 6HCl. Further experimental work has refined the compounds structure with electron energy-loss spectrum analysis[73] and demonstrated a way of producing the material in large quantities *via* thermolysis of the aromatic boron compound 1,3-bis(dibromoboryl)benzene.[74] The results indicate that g-BC_3 features a uniform ordering of B atoms within turbostratically disordered layers.[74]

Sun *et al.*[75] found g-BC_3 (Fig. 5(a)) to be dynamically unstable in LDA calculations and constructed several more stable, up to 22 meV per atom, derivatives. We also observed a full phonon branch along Γ–A to have imaginary frequencies and examined the stability and symmetry of structures derived from g-BC_3 (see Fig. S3, ESI†). An interlayer shift leading to an orthorhombic e-BC_3 polymorph with an oS32 (*Fmmm*) unit cell lowered the energy by 15 meV per atom and eliminated the dynamical instability at Γ but left imaginary frequency modes at the Y point in our optB86b-vdW simulations (Fig. S3, ESI†). By randomly distorting g-BC_3 and performing full unit cell optimizations, we obtained a low-symmetry aP16 ($P\bar{1}$) variant, r-BC_3, 3 meV per atom below e-BC_3 but still dynamically unstable. It is evident that the energy landscape has numerous nearly degenerate minima corresponding to different layered sequences with large unit cells, which is consistent with the experimentally observed stacking disorder.

The discovery of the layered g-BC_3 has offered possibilities of creating a MgB_2-type hole-doped superconductor[76] or a battery anode for high-capacity Li-ion storage.[74,77–79] Given a well-known pressure-induced sp^2 to sp^3 transformation pathway in pure carbon, g-BC_3 was also proposed to serve as a precursor for making a superhard t-BC_3 diamond analog, shown to be enthalpically favored above 4 GPa.[46] Zinin *et al.* did obtain a dense BC_3 polymorph by heating the starting layered material to 2033 K at 50 GPa[22] but its precise structure proved difficult to determine. Several low-enthalpy decorations of the diamond structure were identified with particle swarm optimizations in follow-up studies[72,80] such as (a–c)-BC_3 shown in Fig. 5(d)–(f). Simulated X-ray diffraction (XRD) and Raman peaks for the lowest-enthalpy cubic c-BC_3 phase at $\sim$40 GPa were shown to be in excellent agreement with the experimental data.[80] It is worth noting that none of the polymorphs become truly thermodynamically

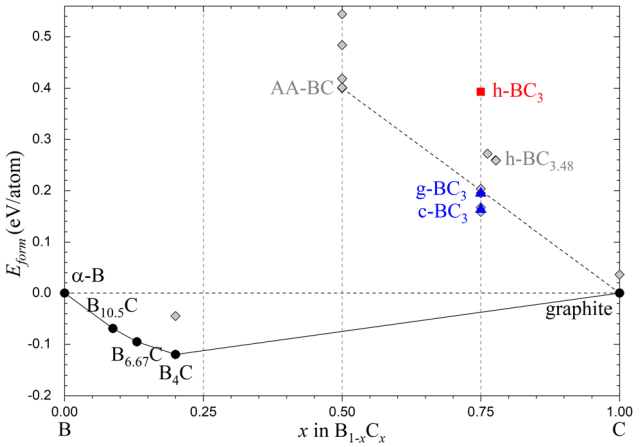

Fig. 6 Calculated formation energies for considered B–C phases. The known $B_{4+\delta}C$ is represented with three related B-rich stable structures (black circles). The reported BC_3 polymorphs are divided into metastable (blue triangles) and unstable (red square). Hypothetical unstable phases, *e.g.*, the layered AA-BC and h-$BC_{3.48}$, are included for reference (gray diamonds).

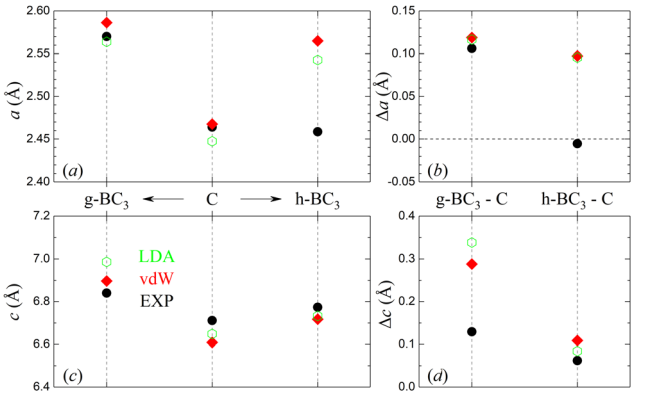

Fig. 7 (a) and (c) Comparison of lattice constants in graphite and BC_3 polymorphs extracted from XRD data and evaluated with different DFT functionals in this work. The experimental values are taken from ref. 74 and 81 for g-BC_3 and from ref. 10 for h-BC_3 and graphite. (b) and (d) Change in the lattice constants in g-BC_3 and h-BC_3 with respect to those in graphite.

stable under compression, *e.g.*, their formation enthalpies with respect to γ-B and diamond-C are over +160 meV per atom at 40 GPa. At ambient pressure, a-BC_3 has the lowest energy among all configurations considered in previous and present studies (see Table S1, ESI†).

In 2018, Milashius *et al.* reported the synthesis of a novel hybrid layered BC_3 phase (h-BC_3) comprised of alternating carbon and borocarbide honeycomb layers.[10] The samples were prepared by heating pure elements to 1200 °C followed by rapid cooling and annealing at 400 °C. Using powder XRD and the Rietveld method, the authors described the material with an ordered $P\bar{6}m2$ hP4 structure shown in Fig. 5(b). The following examination highlights a few inconsistencies of the proposed model.

First, h-BC_3 has a large positive formation energy of over 400 meV per atom. To put it into context, we simulated different stackings of ordered 1 : 1 borocarbide layers and plotted a tie-line connecting the most favorable, albeit dynamically unstable, AA configuration and graphite in Fig. 6. The closeness of the metastable g-BC_3 formation energy to the interpolated value reflects the structure's capacity to accommodate the B–C and C–C bonds with near-optimal lengths, 1.57 Å and 1.42 Å obtained for BC and graphite, respectively (Fig. 5(b)). In contrast, h-BC_3 constraints these covalent bonds to a common intermediate value of 1.48 Å. Our results in Fig. S4 (ESI†) illustrate that a substantial portion of the excess 200 meV per atom corresponds to the elastic energy stored in the compressed B–C and stretched C–C bonds. To illustrate that most of the energy could be released without breaking the covalent bonds within the bulk of h-BC_3, we constructed related hybrid structures with natural bond lengths by combining rotated graphite and heterographite supercells. The hP112 structure shown in Fig. 5(c) with $(6\vec{a} + \vec{b}; -\vec{a} + 5\vec{b})$ and $(5\vec{a}; 5\vec{b})$ lateral expansions of the C and BC hexagonal two-atom unit cells ensures a match within 0.15% between the two unrelaxed sublattices, which makes the resulting off-stoichiometric h-$BC_{3+0.48}$ phase significantly less unstable (Fig. 6). In addition, h-BC_3 was found to be dynamically unstable and feature multiple modes with imaginary frequencies, *e.g.*, $34i$ cm^{-1} at Γ and $396i$ cm^{-1} at M points. These findings indicate that the h-BC_3 formation from pure B and C would not be favored either thermodynamically or kinetically.

Second, the 2.4586 Å in-plane lattice constant extracted from powder XRD data for h-BC_3 appears to be unphysically small, given that the corresponding value for graphite is 2.466 Å.[10] Substitution of a quarter of C atoms for larger B atoms should lead to a noticeable expansion of the lattice, regardless of whether the minority species is distributed in every (g-BC_3) or every other (h-BC_3) layer. We compare the lattice constant change relative to pure graphite in Fig. 7 to reduce the value of known 1–2% systematic DFT errors in the evaluation of bond lengths. According to our optB86b-vdW and LDA results, the in-plane dimensions in both borocarbide structures expand by about 4% reaching 2.586 Å in g-BC_3 with the former functional. Unfortunately, no ($hk0$) peaks have been observed in g-BC_3 bulk samples due to stacking disorder[74] and the only information about the in-plane dimensions was obtained with scanning tunneling microscopy for BC_3 monolayers on NbB_3 (0001).[81,82] The non-strained 2D monolayer (denoted as s-BC_3 in ref. 82 incommensurate with the underlying substrate was found to have a_{C-C} = 1.42 Å, a_{B-C} = 1.55 Å, and a = 2.57 Å consistent with our optimized values. The interlayer distances defined by the weak dispersive interactions are harder to reproduce with (semi)local DFT approximations[83–85] and match experimental values within 1–2% with the employment of vdW functionals. The elongation of the c-axis to 6.77 Å in h-BC_3 noted in ref. 10 is actually less pronounced than the measured and calculated values in g-BC_3 (Fig. 7(d)). In fact, turbostratic forms of graphite obtained *via* heat treatment or ball milling have been reported to have larger c-axis values reaching 6.88 Å.[86,87] Fig. S5 (ESI†) compares the positions and shapes of the key powder XRD peaks observed for the layered carbon and borocarbide materials. The h-BC_3 pattern[10] stands out in that it has relatively sharp

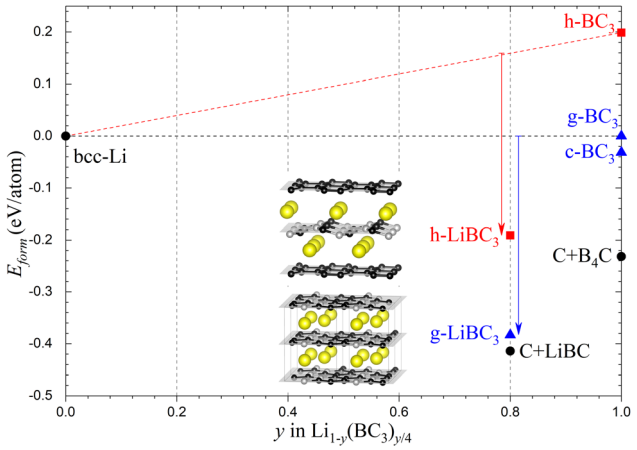

Fig. 8 Relative energies of intercalated $LiBC_3$ phases with respect to bcc-Li and g-BC_3. The solid points at y = 0.8 and y = 1.0 represent the convex hull energies for 2/5C + 3/5LiBC and 11/16C + 5/16B_4C mixtures, respectively.

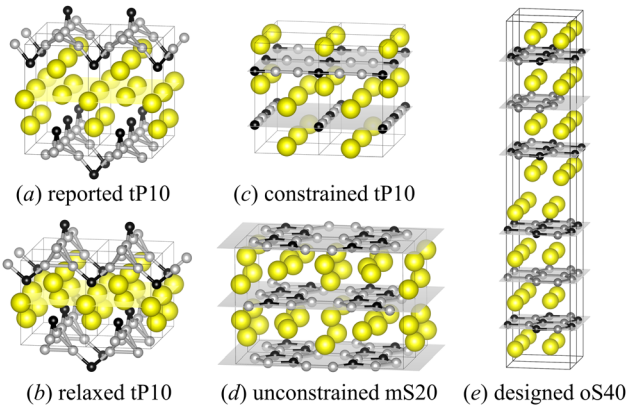

Fig. 9 Crystal structures of select Li_2B_2C phases labeled with Pearson symbols. The Li, B, and C atoms are shown with yellow, gray, and black spheres, respectively. The methods used to construct the polymorphs are detailed in the main text and Fig. 10.

peaks, includes reflections dependent on the in-plane lattice constant, and contains no significant signal from ordered graphite.

We conclude that while the layered h-BC_3 model proposed by Milashius *et al.* provides a reasonable fit to their powder XRD data and is consistent with the 1 : 3 composition established with a microprobe analysis,[10] it is deficient from the thermodynamic or chemical bonding points of view. More experimental information is needed to solve the intriguing new material prepared at this composition.

3.3 $LiBC_3$

Borocarbides with lighter, larger, electron-deficient networks have been considered as promising alternatives to graphite for Li-ion battery applications. Intercalation of boron-substituted B_zC_{1-z} graphite ($z \approx 0.16$) and deintercalation of the stoichiometric LiBC have indeed offered an increased reversible specific capacity of 437 mA h g^{-1} and 450 mA h g^{-1}, respectively.[47,88] First-principles calculations showed that g-BC_3 could accommodate up to $Li_{1.5}$ per formula unit, which corresponds to a theoretical storage capacity of 857 mA h g^{-1}.[78,79] King *et al.*'s experimental study on the g-BC_3 intercalation observed a 700 mA h g^{-1} irreversible Li uptake upon the first charge and a 374 mA h g^{-1} cycling reversibility, presumably between $Li_{0.65}BC_3$ and $Li_{1.5}BC_3$ compositions.[74]

The $LiBC_3$ compound synthesized by Milashius *et al.* directly from the elements was determined with powder and single-crystal XRD measurements to have a hexagonal unit cell with the $P\bar{6}m2$ symmetry and an ordered distribution of atoms in alternating C–C and B–C layers.[11] We approximated the reported lithium borocarbides featuring partial occupation of Li sites[11,74] with small ordered g-$LiBC_3$ (oP10) and h-$LiBC_3$ (oP10) structures shown in Fig. 8 (for comparison, a hexagonal hP15 polymorph was found to be 24 meV per atom less stable than the orthorhombic one for h-$LiBC_3$).

The relative stability results shown in Fig. 8 reveal that the g and h forms of $LiBC_3$ are below the corresponding Li ↔ g-BC_3 and Li ↔ h-BC_3 tie lines by similar 0.38 eV per atom and 0.35 eV per atom margins, respectively. While the Li intercalation brings g-$LiBC_3$ close to true thermodynamic stability (within 31 meV per atom), it does not help h-$LiBC_3$ overcome the energy penalty inherited from the h-BC_3 parent structure. The oP10 model of h-$LiBC_3$ is also dynamically unstable. Therefore, our conclusions on the thermodynamic and kinetic feasibility of the hybrid morphology for BC_3 apply for the lithiated derivatives as well. The disagreement between experimental (2.5408 Å) and DFT (2.5981 Å) in-plane lattice constants in h-$LiBC_3$ is less pronounced (2.2%) than in h-BC_3 (4.1%, see Fig. 7), but still at the higher end of typical systemic DFT errors.

3.4 Li_2B_2C

Pavlyuk *et al.* observed the formation of a new Li_2B_2C compound after a mixture of the elements at the nominal composition was heated at 1473 K and rapidly cooled to room temperature.[9] Collected powder XRD results did not match patterns of any known Li–B–C phases. Based on single-crystal data, the authors proposed a tetragonal structure with space group $P\bar{4}m2$ shown in Fig. 9(a). However, our analysis of the thermodynamic stability and chemical bonding of tP10-Li_2B_2C reveals several issues with the reported solution.

First, the local relaxation of the original structure changed the base lattice constants by less than 0.4% but resulted in a dramatic 25% collapse of the c-axis, from 7.1055 Å to 5.342 Å. While large interlayer spacing mismatches between experiment and (semi)local DFT approximations have been observed for van der Waals solids,[83–85] the comparable results obtained in the LDA (22%) and PBE (25%) treatments make the systematic DFT errors an unlikely source for the discrepancy. Moreover, the 2.6 eV $Å^{-1}$ starting atomic forces and the ensuing 0.33 eV per atom stabilization are too large to be attributed to the typical 1–2% DFT systematic errors for covalent or metallic bond lengths.

Pavlyuk *et al.* made an interesting comparison between the connectivity of building blocks in the proposed tP10-Li_2B_2C and

in several known compounds.[9] However, the 2D display of the atomic arrangements and the reference to the units as B_4 and B_2C_2 squares do not reflect the true 3D connectivity of the covalent frameworks in the YB_2C_2, CrB_4,‡ CeB_2C_2, LiB_3, and ThB_4 compounds featuring octahedra and diamond-like local environments. In fact, a visual examination of the original tP10 structure in Fig. 9(a) reveals that the C and B atoms in the corrugated networks are actually undercoordinated, having only two and three neighbors within 1.9 Å, respectively. The local optimization brings an additional neighbor within the effective interaction range for B but cannot improve the atypical local environment with a dangling bond for C (Fig. 9(b)). It leaves the structure 0.437 eV per atom above the convex hull (Fig. 3) and dynamically unstable, with imaginary frequencies as high as $198i$ cm^{-1} across the Brillouin zone.

Next, we attempted to find more stable Li_2B_2C polymorphs using our evolutionary algorithm. We started by constraining our searches to the reported unit cell dimensions and the $P\bar{4}m2$ space group. The inclusion of prior information extracted from experiment is known to accelerate the identification of ground states by 2–3 orders of magnitude.[89] These constrained evolutionary runs did produce an alternative tP10 structure with lower energy (by 66 meV per atom after full unit cell relaxation), higher symmetry ($P4_2/mmc$), and conspicuously different morphology with crisscrossing B_2C linear chains (Fig. 9(c)). Given the difficulty of determining the exact atomic positions of light elements in XRD measurements and the significant reduction of volume upon relaxation of the original tP10 structure, we also tried to fit three Li_2B_2C formula units (15 atoms) into the reported unit cell but the best candidate turned out to be suboptimal. Additional runs with 10–15 atoms per unit cell and compositions near 2 : 2 : 1 did not produce viable Li–B–C phases with the $P\bar{4}m2$ symmetry.

We proceeded with unconstrained evolutionary searches initialized with random configurations. The global optimization uncovered substantially more stable polymorphs. Runs with two formula units yielded the best mS20 structure with an interesting layered morphology. As can be seen in Fig. 9(d), the three-fold connectivity satisfying the Eulers rule[90] is maintained *via* the combination two pentagons and one octagon rather than three hexagons. The B_2C framework enabling sp^2 bonding makes mS20 more stable by over 200 meV per atom compared to the other candidates (Fig. 10). Searches with larger system sizes did not produce better configurations; the fact that our extensive runs with four formula units did not reproduce the energy of the best candidates with two formula units highlights the difficulty of finding complex stable configurations with 20 atoms.

Finally, we relied on general knowledge of favorable motifs in M–B and M–B–C materials to manually construct better polymorphs. The title compound can be thought of a combination of $(LiB)_2$ and C materials known to be stable as stackings

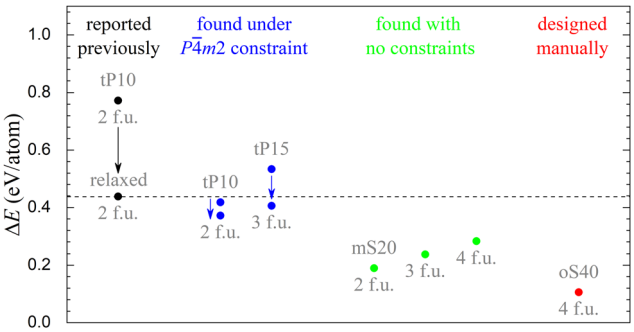

Fig. 10 Distance to the convex hull for Li_2B_2C competing structures reported previously[9] and identified in this study. The size of the unit cell is specified with the number of formula units (f.u.). The arrows indicate the energies before and after the full relaxation of the lattice parameters.

of honeycomb covalent networks.[15] As discussed in the case of BC_3, the B- and C-based layers are too different in size to be combined as separate units. Mixing B and C within the LiB structure would not maintain the desired composition. Therefore, we examined a hybrid LiB-MgB_2 structure introduced in our previous study[3] and sampled different decorations of the B/C sites. The resulting oS40 structure shown in Fig. 9(e) proved to be a significantly more stable configuration. Because of the large c/a ratio, standard evolutionary operations could not create it. Despite being our best guess at this composition, oS40 remains 105 meV per atom above the convex hull (Fig. 10) and is not expected to form.

4 Conclusions

The presented *ab initio* analysis further elucidates the interplay between thermodynamic and kinetic factors governing the formation of Li–B–C compounds. Whereas the observed delithiated Li_xBC ($x > 0.38$) phases and BC_3 (g and c) polymorphs are known to be only metastable under ambient conditions, our results indicate that they are metastable under synthesis conditions as well. In case of Li_xBC, the delithiation process is driven by the high entropy of Li_2^{gas} at elevated temperatures while the strongly bonded BC layers prevent the material's decomposition into other products, *e.g.*, Li_2^{gas} + C + B_4C. Our constructed *ab initio* (T,P) phase diagram is in good agreement with previous observations.[5,7] For BC_3, the synthesis of sp^2 and sp^3 compounds relies on natural rebonding pathways between precursor and targeted materials. On the other hand, reported h-BC_3, h-$LiBC_3$, and Li_2B_2C phases obtained from the elements[9–11] have been shown to have unnatural structural features and high positive formation energies. We hope that our findings will stimulate further synthesis and characterization work on this interesting materials class.

Conflicts of interest

There are no conflicts to declare.

‡ Ref. 9 displayed a previously misidentified oI10 crystal structure for CrB_4. The compound was predicted[93] and confirmed[94] to have a lower-symmetry oP10 ground state structure with a significantly distorted 3D boron framework.

Acknowledgements

The authors acknowledge support from the National Science Foundation (NSF) (Awards no. DMR-2132586 and DMR-2132589). This work used the Expanse system at the San Diego Supercomputer Center *via* allocation TG-DMR180071 and the Frontera supercomputer at the Texas Advanced Computing Center *via* the Leadership Resource Allocation (LRAC) award DMR22004. Expanse is supported by the Extreme Science and Engineering Discovery Environment (XSEDE) program[91] through NSF award no. ACI-1548562, and Frontera is supported by NSF award no. OAC-1818253.[92]

Notes and references

1 F. Thevenot, *J. Eur. Ceram. Soc.*, 1990, **6**, 205–225.
2 J. Asenbauer, T. Eisenmann, M. Kuenzel, A. Kazzazi, Z. Chen and D. Bresser, *Sustainable Energy Fuels*, 2020, **4**, 5387–5416.
3 G. P. Kafle, C. R. Tomassetti, I. I. Mazin, A. N. Kolmogorov and E. R. Margine, *Phys. Rev. Mater.*, 2022, **6**, 084801.
4 H. Rosner, A. Kitaigorodsky and W. E. Pickett, *Phys. Rev. Lett.*, 2002, **88**, 127001.
5 L. Zhao, P. Klavins and K. Liu, *J. Appl. Phys.*, 2003, **93**, 8653–8655.
6 A. M. Fogg, J. B. Claridge, G. R. Darling and M. J. Rosseinsky, *Chem. Commun.*, 2003, 1348–1349.
7 A. M. Fogg, J. Meldrum, G. R. Darling, J. B. Claridge and M. J. Rosseinsky, *J. Am. Chem. Soc.*, 2006, **128**, 10043–10053.
8 B. Kalkan and E. Ozdas, *ACS Appl. Mater. Interfaces*, 2019, **11**, 4111–4122.
9 V. Pavlyuk, V. Milashys, G. Dmytriv and H. Ehrenberg, *Acta Crystallogr., Sect. C: Struct. Chem.*, 2015, **71**, 39–43.
10 V. Milashius, V. Pavlyuk, G. Dmytriv and H. Ehrenberg, *Inorg. Chem. Front.*, 2018, **5**, 853–863.
11 V. Milashius, V. Pavlyuk, K. Kluziak, G. Dmytriv and H. Ehrenberg, *Acta Crystallogr., Sect. C: Struct. Chem.*, 2017, **73**, 984–989.
12 A. Van Der Geest and A. Kolmogorov, *Calphad*, 2014, **46**, 184–204.
13 M. Wörle and R. Nesper, *Angew. Chem., Int. Ed.*, 2000, **39**, 2349–2353.
14 A. N. Kolmogorov and S. Curtarolo, *Phys. Rev. B: Condens. Matter Mater. Phys.*, 2006, **74**, 224507.
15 A. N. Kolmogorov and S. Curtarolo, *Phys. Rev. B: Condens. Matter Mater. Phys.*, 2006, **73**, 180501.
16 A. Kolmogorov, S. Hajinazar, C. Angyal, V. Kuznetsov and A. Jephcoat, *Phys. Rev. B: Condens. Matter Mater. Phys.*, 2015, **92**, 144110.
17 M. S. Dresselhaus and G. Dresselhaus, *Adv. Phys.*, 2002, **51**, 1–186.
18 J. Sangster, *J. Phase Equilib. Diffus.*, 2007, **28**, 561–570.
19 Y. Lin, T. A. Strobel and R. E. Cohen, *Phys. Rev. B: Condens. Matter Mater. Phys.*, 2015, **92**, 214106.
20 P. F. Rogl, J. Vřešťál, T. Tanaka and S. Takenouchi, *Calphad*, 2014, **44**, 3–9.
21 J. Kouvetakis, R. B. Kaner, M. L. Sattler and N. Bartlett, *J. Chem. Soc., Chem. Commun.*, 1986, 1758–1759.
22 P. V. Zinin, L. C. Ming, I. Kudryashov, N. Konishi and S. K. Sharma, *J. Raman Spectrosc.*, 2007, **38**, 1362–1367.
23 N. Vojteer and H. Hillebrecht, *Angew. Chem., Int. Ed.*, 2006, **45**, 165–168.
24 M. Wörle, R. Nesper, G. Mair, M. Schwarz and H. G. Von Schnering, *Z. fur Anorg. Allg. Chem.*, 1995, **621**, 1153–1159.
25 A. Jay, O. Hardouin Duparc, J. Sjakste and N. Vast, *J. Appl. Phys.*, 2019, **125**, 185902.
26 G. Kresse and J. Hafner, *Phys. Rev. B: Condens. Matter Mater. Phys.*, 1993, **47**, 558–561.
27 G. Kresse and J. Hafner, *Phys. Rev. B: Condens. Matter Mater. Phys.*, 1994, **49**, 14251–14269.
28 G. Kresse and J. Furthmüller, *Comput. Mater. Sci.*, 1996, **6**, 15–50.
29 G. Kresse and J. Furthmüller, *Phys. Rev. B: Condens. Matter Mater. Phys.*, 1996, **54**, 11169–11186.
30 H. J. Monkhorst and J. D. Pack, *Phys. Rev. B: Solid State*, 1976, **13**, 5188–5192.
31 J. Klimeš, D. R. Bowler and A. Michaelides, *Phys. Rev. B: Condens. Matter Mater. Phys.*, 2011, **83**, 195131.
32 J. P. Perdew, K. Burke and M. Ernzerhof, *Phys. Rev. Lett.*, 1996, **77**, 3865–3868.
33 D. C. Langreth and M. J. Mehl, *Phys. Rev. B: Condens. Matter Mater. Phys.*, 1983, **28**, 1809–1834.
34 D. M. Ceperley and B. J. Alder, *Phys. Rev. Lett.*, 1980, **45**, 566.
35 J. P. Perdew and A. Zunger, *Phys. Rev. B: Condens. Matter Mater. Phys.*, 1981, **23**, 5048.
36 S. Hajinazar, A. Thorn, E. D. Sandoval, S. Kharabadze and A. N. Kolmogorov, *Comput. Phys. Commun.*, 2021, **259**, 107679.
37 A. Togo and I. Tanaka, *Scr. Mater.*, 2015, **108**, 1–5.
38 P. Ravindran, P. Vajeeston, R. Vidya, A. Kjekshus and H. FjellvÅg, *Phys. Rev. B: Condens. Matter Mater. Phys.*, 2001, **64**, 224509.
39 A. Bharathi, S. J. Balaselvi, M. Premila, T. Sairam, G. Reddy, C. Sundar and Y. Hariharan, *Solid State Commun.*, 2002, **124**, 423–428.
40 D. Souptel, Z. Hossain, G. Behr, W. Löser and C. Geibel, *Solid State Commun.*, 2003, **125**, 17–21.
41 Y. Nakamori and S. ichi Orimo, *J. Alloys Compd.*, 2003, **370**, L7–L9.
42 Q. Xu, C. Ban, A. C. Dillon, S.-H. Wei and Y. Zhao, *J. Phys. Chem. Lett.*, 2011, **2**, 1129–1132.
43 J. An, *Phys. B*, 2003, **328**, 1–5.
44 K.-W. Lee and W. E. Pickett, *Phys. Rev. B: Condens. Matter Mater. Phys.*, 2003, **68**, 085308.
45 S. Lebègue, B. Arnaud, P. Rabiller, M. Alouani and W. E. Pickett, *Europhys. Lett.*, 2004, **68**, 846–852.
46 Z. Li Liu, X.-R. Chen and Y.-L. Wang, *Phys. B*, 2006, **381**, 139–143.
47 D. Li, P. Dai, Y. Chen, R. Peng, Y. Sun and H. Zhou, *J. Phys. Chem. C*, 2018, **122**, 18231–18236.
48 P. C. Ellgen, Thermodynamics and Chemical Equilibrium, 2014, https://chem.libretexts.org/Bookshelves/Physical_and_Theoretical_Chemistry_Textbook_Maps/Book.
49 K. F. Dziubek, *Crystals*, 2022, **12**, 1186.

50 A. I. Boldyrev, J. Simons and P. v R. Schleyer, *J. Chem. Phys.*, 1993, **99**, 8793–8804.
51 E. Joseph and M. Haque, *Asian J. Phys. Chem. Sci.*, 2016, **1**, 1–10.
52 S. Kharabadze, A. Thorn, E. A. Koulakova and A. N. Kolmogorov, *npj Comput. Mater.*, 2022, **8**, 136.
53 P. B. Allen, *Mod. Phys. Lett. B*, 2020, **34**, 2050025.
54 M. M. Hessel and C. Vidal, *J. Chem. Phys.*, 1979, **70**, 4439–4459.
55 B. Monserrat, N. D. Drummond and R. J. Needs, *Phys. Rev. B: Condens. Matter Mater. Phys.*, 2013, **87**, 144302.
56 T. Tadano and S. Tsuneyuki, *J. Ceram. Soc. Jpn.*, 2019, **127**, 404–408.
57 R. P. Elliott, 1965, 877 P. Mcgraw-Hill Book Bo., 330 W. 42nd St New York, N. Y. 10036, 1965.
58 C. Lowell, *J. Am. Ceram. Soc.*, 1967, **50**, 142–144.
59 K. Ploog, *J. Less-Common Met.*, 1974, **35**, 115–130.
60 K. Ploog, *J. Less-Common Met.*, 1974, **35**, 131–145.
61 K. Ploog, *J. Electrochem. Soc.*, 1974, **121**, 846.
62 T. L. Aselage and D. Emin, *AIP Conf. Proc.*, 1991, 177–185.
63 T. L. Aselage and R. G. Tissot, *J. Am. Ceram. Soc.*, 1992, **75**, 2207–2212.
64 D. N. Kevill, T. J. Rissmann, D. Brewe and C. Wood, *J. Cryst. Growth*, 1986, **74**, 210–216.
65 G. Will, A. Kirfel, A. Gupta and E. Amberger, *J. Less-Common Met.*, 1979, **67**, 19–29.
66 H. K. Clark and J. L. Hoard, *J. Am. Chem. Soc.*, 1943, **65**, 2115–2119.
67 B. Morosin, A. W. Mullendore, D. Emin and G. A. Slack, *AIP Conf. Proc.*, 1986, **140**, 70–86.
68 R. Lazzari, N. Vast, J. Besson, S. Baroni and A. Dal Corso, *Phys. Rev. Lett.*, 1999, **83**, 3230.
69 F. Mauri, N. Vast and C. J. Pickard, *Phys. Rev. Lett.*, 2001, **87**, 085506.
70 M. Calandra, N. Vast and F. Mauri, *Phys. Rev. B: Condens. Matter Mater. Phys.*, 2004, **69**, 224505.
71 D. Bylander, L. Kleinman and S. Lee, *Phys. Rev. B: Condens. Matter Mater. Phys.*, 1990, **42**, 1394.
72 H. Liu, Q. Li, L. Zhu and Y. Ma, *Phys. Lett. A*, 2011, **375**, 771–774.
73 K. M. Krishnan, *Appl. Phys. Lett.*, 1991, **58**, 1857–1859.
74 T. C. King, P. D. Matthews, H. Glass, J. A. Cormack, J. P. Holgado, M. Leskes, J. M. Griffin, O. A. Scherman, P. D. Barker, C. P. Grey, S. E. Dutton, R. M. Lambert, G. Tustin, A. Alavi and D. S. Wright, *Angew. Chem., Int. Ed.*, 2015, **127**, 6017–6021.
75 H. Sun, F. J. Ribeiro, J.-L. Li, D. Roundy, M. L. Cohen and S. G. Louie, *Phys. Rev. B: Condens. Matter Mater. Phys.*, 2004, **69**, 024110.
76 F. J. Ribeiro and M. L. Cohen, *Phys. Rev. B: Condens. Matter Mater. Phys.*, 2004, **69**, 212507.
77 A. A. Kuzubov, A. S. Fedorov, N. S. Eliseeva, F. N. Tomilin, P. V. Avramov and D. G. Fedorov, *Phys. Rev. B: Condens. Matter Mater. Phys.*, 2012, **85**, 195415.
78 Y. Liu, V. I. Artyukhov, M. Liu, A. R. Harutyunyan and B. I. Yakobson, *J. Phys. Chem. Lett.*, 2013, **4**, 1737–1742.
79 R. P. Joshi, B. Ozdemir, V. Barone and J. E. Peralta, *J. Phys. Chem. Lett.*, 2015, **6**, 2728–2732.
80 M. Zhang, H. Liu, Q. Li, B. Gao, Y. Wang, H. Li, C. Chen and Y. Ma, *Phys. Rev. Lett.*, 2015, **114**, 015502.
81 A. Ueno, T. Fujita, M. Matsue, H. Yanagisawa, C. Oshima, F. Patthey, H.-C. Ploigt, W.-D. Schneider and S. Otani, *Surf. Sci.*, 2006, **600**, 3518–3521.
82 H. Yanagisawa, Y. Ishida, T. Tanaka, A. Ueno, S. Otani and C. Oshima, *Surf. Sci.*, 2006, **600**, 4072–4076.
83 A. N. Kolmogorov and V. H. Crespi, *Phys. Rev. B: Condens. Matter Mater. Phys.*, 2005, **71**, 235415.
84 G. Graziano, J. Klimeš, F. Fernandez-Alonso and A. Michaelides, *J. Phys.: Condens. Matter*, 2012, **24**, 424216.
85 O. Lenchuk, P. Adelhelm and D. Mollenhauer, *J. Comput. Chem.*, 2019, **40**, 2400–2412.
86 V. Bayot, L. Piraux, J.-P. Michenaud, J.-P. Issi, M. Lelaurain and A. Moore, *Phys. Rev. B: Condens. Matter Mater. Phys.*, 1990, **41**, 11770–11779.
87 Z. Li, C. Lu, Z. Xia, Y. Zhou and Z. Luo, *Carbon*, 2007, **45**, 1686–1695.
88 B. M. Way and J. R. Dahn, *J. Electrochem. Soc.*, 1994, **141**, 907–912.
89 A. Kolmogorov, S. Shah, E. Margine, A. Kleppe and A. Jephcoat, *Phys. Rev. Lett.*, 2012, **109**, 075501.
90 E. R. Margine, A. N. Kolmogorov, D. Stojkovic, J. O. Sofo and V. H. Crespi, *Phys. Rev. B: Condens. Matter Mater. Phys.*, 2007, **76**, 115436.
91 J. Towns, T. Cockerill, M. Dahan, I. Foster, K. Gaither, A. Grimshaw, V. Hazlewood, S. Lathrop, D. Lifka, G. D. Peterson, R. Roskies, J. R. Scott and N. Wilkins-Diehr, *Comput. Sci. Eng.*, 2014, **16**, 62–74.
92 D. Stanzione, J. West, R. T. Evans, T. Minyard, O. Ghattas and D. K. Panda, *Frontera: The Evolution of Leadership Computing at the National Science Foundation*, ACM, New York, NY, USA, 2020, pp. 106–111.
93 A. F. Bialon, T. Hammerschmidt, R. Drautz, S. Shah, E. R. Margine and A. N. Kolmogorov, *Appl. Phys. Lett.*, 2011, **98**, 081901.
94 H. Niu, J. Wang, X.-Q. Chen, D. Li, Y. Li, P. Lazar, R. Podloucky and A. N. Kolmogorov, *Phys. Rev. B: Condens. Matter Mater. Phys.*, 2012, **85**, 144116.

